Proceedings World Geothermal Congress 2015
Melbourne, Australia, 19-25 April 2015

Predicting the Channeling Flows through Fractures at Various Scales

Noriaki Watanabe[1], Takuya Ishibashi[2] and Noriyoshi Tsuchiya[1]

1. Graduate School of Environmental Studies, Tohoku University, 6-6-20 Aramaki-aza-Aoba, Aoba-ku, Sendai 980-8579, Japan

watanabe@mail.kankyo.tohoku.ac.jp; tsuchiya@mail.kankyo.tohoku.ac.jp

2. Fukushima Renewable Energy Institute, AIST, 2-2-9 Machiike-dai, Koriyama, Fukushima 963-0215, Japan

takuya.ishibashi@aist.go.jp

Keywords: scale dependency; channeling flow; fracture; permeability; confining stress; shear displacement

ABSTRACT

The present study evaluates aperture distributions and fluid flow characteristics for variously sized laboratory scale granite fractures under confining stress. As a significant result, the contact area in the fracture plane was found to be independent of scale. By combining this characteristic with the fractal nature of the fracture surfaces, a method for predicting fracture aperture distributions beyond laboratory scale is developed. The validity of the method is revealed through reproduction of the results of the laboratory investigation and the maximum aperture-fracture length relations, which have been reported in the literature. The present study finally predicts conceivable scale dependencies of fluid flows through joints and faults (fractures without and with shear displacement). Both joint and fault aperture distributions are characterized by a scale-independent contact area, a scale-dependent geometric mean, and a scale-independent geometric standard deviation of the aperture. The contact areas for joints and faults are approximately 60% and 40%, respectively. The changes in the geometric means of joint and fault apertures (μm), $e_{m,\ joint}$ and $e_{m,\ fault}$, with fracture length (m), l, are respectively approximated by $e_{m,\ joint} = 1\times10^{2}l^{0.1}$ and $e_{m,\ fault} = 1\times10^{3}l^{0.7}$, whereas the geometric standard deviations of both joint and fault apertures are approximately 3. Fluid flows through both joints and faults are characterized by the formations of preferential flow paths (channeling flows) with scale-independent flow areas of approximately 10%, whereas the joint and fault permeabilities (m^2), k_{joint} and k_{fault}, are scale dependent and are approximated as $k_{joint} = 1\times10^{-12}l^{0.2}$ and $k_{fault} = 1\times10^{-8}l^{1.1}$, respectively.

1. INTRODUCTION

Fluid flow and related transport characteristics in rock fracture networks are of critical interest in numerous engineering and scientific fields, including effective recovery of target fluids, such as geothermal fluids, hydrocarbons, and potable water, as well as safe isolation of hazardous materials. In analyzing fluid flows in fracture networks, discrete fracture network (DFN) model simulations have broad applicability because they can naturally incorporate geometrical properties in fractures (fracture scale, aperture, location, orientation, and density), and as a result can explicitly account for contributions of individual fractures to fluid flow and transport phenomena (Long et al., 1982; Berkowitz, 2002; Neuman, 2005; Dreuzy et al., 2012). In the DFN models, individual fractures are represented by pairs of parallel smooth plates having single aperture values (Jing et al., 2000; Min et al., 2004). However, fractures have heterogeneous aperture distributions because the apertures are formed by pairs of rough surfaces that are in partial contact with each other. Such a heterogeneous aperture distribution of rock fracture is precisely visualized using X-ray CT at atmospheric pressure or under confining stress (Watanabe et al., 2011a, 2011b, and 2012). Fluid flows through fractures have long been recognized to be characterized by the formation of preferential flow paths (i.e., channeling flow) (Brown, 1987b and 1989; Pyrak-Nolte et al., 1988; Brown et al., 1995; Brown et al., 1998; Watanabe et al., 2008; Nemoto et al., 2009; Talon et al., 2010). The occurrence of channeling flows within fractures was examined through field investigations at the Stripe mine in Sweden (Abelin et al., 1985; Tsang and Neretnieks, 1998). Therefore, in the next generation of fracture network model simulators, for better understanding of fluid flow and transport phenomena, explicit consideration of the formation of 3-D preferential flow paths (i.e., 3-D channeling flow) in fracture networks is desirable.

In order to address this concern, the authors have recently developed a novel 3-D fracture network model simulator, namely GeoFlow, in which fractures are characterized by 2-D heterogeneous aperture distributions (Ishibashi et al., 2012). GeoFlow is a hybrid DFN and continuum model simulator to consider combination of fractures having aperture distributions and the matrix, and its availability to analyze 3-D channeling flow in a fracture network has been demonstrated in a laboratory multiple-fracture flow experiment. The limitation of conventional fracture network model simulations and the importance of considering 3-D channeling flows have been clarified. In applying GeoFlow or other simulators, which can consider the impact of 3-D channeling flow, to practical field-scale problems, it is required to understand aperture distributions and resulting fluid flow characteristics for fractures beyond the laboratory scale.

Based on the fluid flow experiments and field investigations, Witherspoon et al. (1979) and Raven and Gale (1985) reported that the scale of the rock fracture may influence its permeability, although their results are inconsistent. Matsuki et al. (2006), on this, suggested that experimentally determining the scale dependency for the permeability of a fracture is difficult because individual samples have unique aperture layouts. Therefore, they investigated the scale dependencies in the aperture and the permeability of fractures both with and without shear displacement using numerically created fractures. Their results have significant advantages in that their investigations were systematic. However, the effect of confining stress on the fracture flow characteristics is not strictly introduced in their evaluation because they assumed constant mean apertures. Furthermore, they never compared the absolute values of the aperture and the permeability with those for actual rock fractures. Thus, predicting the flow characteristics of rock fractures that include natural and artificial fractures remains difficult.

The objectives of the present study are to investigate fluid flows through aperture distributions of fractures of various size under confining stress in the laboratory and to obtain insight into the scale dependencies of the aperture distribution and the resulting fluid flow characteristics beyond laboratory scale, based on laboratory investigations. The present study first evaluates aperture distributions and resulting fluid flow characteristics for granite fractures of up to 0.2 m × 0.3 m at confining stresses up to 30 MPa. Either no shear displacement or a 5-mm shear displacement is assigned the each of the scaled fractures. A novel method by which to predict fracture aperture distributions beyond the laboratory scale is developed based on the evaluations of the present study. This method is verified through the reproduction of the results obtained in the laboratory investigation, as well as the maximum aperture-fracture length relations, which have been reported in the literature, for natural fractures. Finally, the present study predicts conceivable scale dependencies of aperture distributions and fluid flow characteristics of subsurface fractures, such as joints (fractures without shear displacement) and faults (fractures with shear displacement).

2. METHODS

2.1 Evaluation of Fracture Aperture Distributions and Fluid Flows on the Laboratory Scale

The fracture aperture distribution under confining stress and the fluid flow through the aperture distributions are determined using data of the fracture surface topography and permeability, as described in the literature (Watanabe et al., 2008 and 2009). Measurements of the fracture surface topography and permeability are, therefore, conducted on single fractures for scales of 0.05 m × 0.075 m, 0.1 m × 0.15 m, and 0.2 m × 0.3 m. These fractures are contained in cylindrical samples of Inada medium-grained granite (Ibaraki prefecture, Japan), and the diameters and lengths of these samples are equivalent to the short and long side lengths, respectively, of the rectangular fractures. The fracture is a tensile fracture induced by a wedge and has either no shear displacement or a shear displacement of 5 mm in the radial direction. The shear displacement is created by the lateral offset of initially well-mated fracture surfaces that are created in a cubic granite block and is maintained by fixing the fractured granite block with mortar during coring. The surface topography is measured for each fracture before measuring the permeability under confining stress. Two-dimensional distributions of surface height are measured in a 0.25-mm square grid system with a laser profilometer, which has a height resolution of 10 μm and a positioning accuracy of 20 μm. The data for surface topographies are used as input data for the numerical determination of fracture aperture distributions and the fluid flows within the fractures by means of the permeability matching method described later herein.

The permeability for each fracture is measured at confining stresses of 10, 20, and 30 MPa through a unidirectional fluid flow experiment along the sample axis at room temperature. The rubber-sleeved fractured sample is subjected to confining stress (hydrostatic pressure by water) in a pressure vessel. While distilled water flows through the sample at a constant flow rate, a corresponding differential pressure between the inlet and the outlet is measured by a differential pressure gauge. The flow rate is controlled by a water pump and confirmed by measuring the weight of the effluent using an electronic balance. Low pore pressures of less than 5% of the given confining stress are used so that the effective confining stresses do not differ significantly from the confining stress values. Since linear relationships between the flow rate and the differential pressure are observed for all given conditions, the fracture permeability is determined for the sample with a negligible matrix permeability of from 10^{-19} to 10^{-18} m^2 based on the cubic law (Witherspoon et al., 1980; Tsang and Witherspoon, 1981):

$$k = \frac{e_h^2}{12}, \tag{1}$$

where k is the fracture permeability, and e_h is the hydraulic aperture, which is described as follows:

$$e_h = \left(-\frac{12\mu L Q}{W \Delta P} \right), \tag{2}$$

where Q is the flow rate, ΔP is the differential pressure, μ is the viscosity of the fluid, and L and W are the long and short side lengths, respectively, of the fracture.

Based on the measurements of the fracture surface topography and permeability, 2-D aperture distributions of the fractures under the confining stresses are numerically determined by computer through a permeability matching method, in which the pairs of fracture surfaces are in contact with each other, so that the aperture distributions have the experimentally determined fracture permeabilities. In this permeability matching, an aperture distribution with at least a single contact point is first created in the 0.25-mm square grid system, and the apertures are decreased to simulate fracture closure due to confining stress. The apertures are local separations between two opposite fracture surfaces in the direction normal to their mean planes. In decreasing the apertures, the two fracture surfaces become close together and some asperities are overlapped. Overlapping asperities are assumed to be contacting asperities (i.e., regions of zero aperture), and fracture surface deformations are not considered (Zimmerman et al., 1992; Matsuki et al., 2006). The permeability of the aperture distribution is evaluated by simulating a unidirectional fluid flow in a 2-D (x-y) field with the Reynolds equation for a steady-state laminar flow of a viscous and incompressible fluid (Brown, 1987b; Ge, 1997; Oron and Berkowitz, 1998; Yeo et al., 1998; Sausse, 2002; Brush and Thomson, 2003; Jaeger et al., 2007):

$$\frac{\partial}{\partial x}\left(e^3 \frac{\partial P}{\partial x} \right) + \frac{\partial}{\partial y}\left(e^3 \frac{\partial P}{\partial y} \right) = 0 , \tag{3}$$

where e is the aperture, and P is the pressure of the fluid. The Reynolds equation is solved with a finite difference method under the same boundary condition as that in the fluid flow experiment. In solving the Reynolds equation, the contacting asperities are replaced with a negligibly small nonzero aperture of 1 μm because the pressure cannot be defined at zero aperture. Since the fluid

flow simulation mimics the fluid flow experiment, the permeabilities for the aperture distributions are also determined using Equations (1) and (2).

As described later herein, all aperture distributions obtained in the present study are characterized by a significant number of contacting asperities (regions of zero aperture) and the skewed distributions of nonzero apertures with long tails, i.e., lognormal-like distributions. Hence, the aperture distributions are evaluated based on the percentages of contacting asperities for all data points (i.e., contact area), the geometric mean, and the geometric standard deviation of the apertures (nonzero values). In evaluating the fluid flows resulting from the fluid flow simulation for the aperture distributions, the area of preferential flow paths in the fracture plane is evaluated because the fluid flows are always characterized as channeling flows.

2.2 Prediction of Fracture Aperture Distributions and Fluid Flows beyond Laboratory Scale

The results of the laboratory investigation inspired the following novel idea of predicting the aperture distributions of beyond laboratory-scale fractures under confining stress. The fractal nature of fracture surface topography is well known (Brown, 1987a; Power et al., 1987; Kumar and Bodvarsson, 1990; Power and Durham, 1997). Based on the fractal nature, the fracture surface topography can be numerically created (Brown, 1995; Glover et al., 1997 and 1998; Matsuki et al., 2006). Moreover, the fractal nature has been confirmed to be valid for the natural fault roughness from the micro-scale to the continental scale (Candela et al., 2012; Renard et al., 2013). Consequently, a method used to predict the fracture surface topography beyond the laboratory scale has already been developed. Therefore, the only problem in predicting the aperture distributions of fractures beyond the laboratory scale is how closely the two opposite fracture surfaces are situated under confining stress.

Fracture permeability, mean aperture, or contact area may be used to predict the aperture distribution under confining stress, as long as their scale dependencies are clear and formulated. As described later herein, the scale dependencies of fracture permeability and mean aperture are not clear in the laboratory investigation, which precludes the formulation of their scale dependencies. On the other hand, the scale independency of the contact area has been suggested, and a novel method by which to predict the aperture distributions of fractures from a laboratory scale to a field scale has been developed based on the fractal nature of the fracture surface and the scale-independent contact area. In other words, the aperture distribution of a fracture of any size can be predicted by simply placing the two fractal fracture surfaces in contact so that the fracture has the scale-independent contact area.

The method developed by Matsuki et al. (2006) is used in creating a pair of fractal fracture surfaces (upper and lower fracture surfaces). Their method is a modification of the method of Brown (1995) or Glover et al. (1997 and 1998), so that the desired degree of matedness of the two fracture surfaces can be considered. For creating the upper fracture surface, the fractal dimension of the fracture surface, and the standard deviation of the fracture surface height, along a linear profile of reference length are required. In contrast, the mismatch length scale and the ratio of the power spectral density (PSD) of the initial aperture with at least a single contact point to the PSD of the surface height as a function of spatial frequency, $R(f)$, are required in creating the lower fracture surface having the desired degree of matedness with the upper fracture surface. In the present study, the representative parameter values are computed for the fracture surface topographies of the 0.2 m × 0.3 m surface, providing a fractal dimension of 2.3, a standard deviation of 1.3 mm for a reference length of 0.2 m, and a mismatch length scale of 0.7 mm. In addition, the ratio of the PSD of the initial aperture to the PSD of the surface height is approximated by:

$$R(f) = e^{\left\{-6.5\times10^{-3}\cdot(\ln f)^3 - 2.9\times10^{-1}\cdot(\ln f)^2 + 2.2\times10^{-1}\cdot(\ln f) + 5.5\times10^{-1}\right\}}. \quad (4)$$

With these parameter values, pairs of surface topographies of square fractures on a 0.25-mm square grid system are numerically created on a scale of from 0.05 m × 0.05 m to 0.6 m × 0.6 m. Aperture distributions having a scale-independent contact area are then determined and evaluated as described earlier herein. Then, the fluid flows through the predicted aperture distributions are determined and evaluated. The present study essentially provides results for factures beyond the laboratory scale, because even the present maximum fracture size is too large to experimentally determine its aperture distribution and corresponding fluid flow under confining stress.

3. RESULTS AND DISCUSSION

3.1 Channeling Flows through Heterogeneous Aperture Distributions of Laboratory Scale Fractures

The results of the permeability measurement for the laboratory scale fractures reveal different changes in permeability with fracture scale between the fractures with and without shear displacement (Figure 1). Note that the scales for the rectangular laboratory-scale fractures in the following figures are represented by the shorter side lengths. For the case of a fracture without shear displacement, the permeability, which has a lower value at a higher confining stress, increases with the fracture length from 0.05 m to 0.1 m and decreases with the increase in the fracture length from 0.1 m to 0.2 m at all given confining stresses. Consequently, the permeability for the fracture without shear displacement shows no clear scale dependency. On the other hand, the permeability of the fracture with shear displacement, which is much higher than that of the fracture without shear displacement, increases with the fracture length, where no significant change in permeability with confining stress is observed.

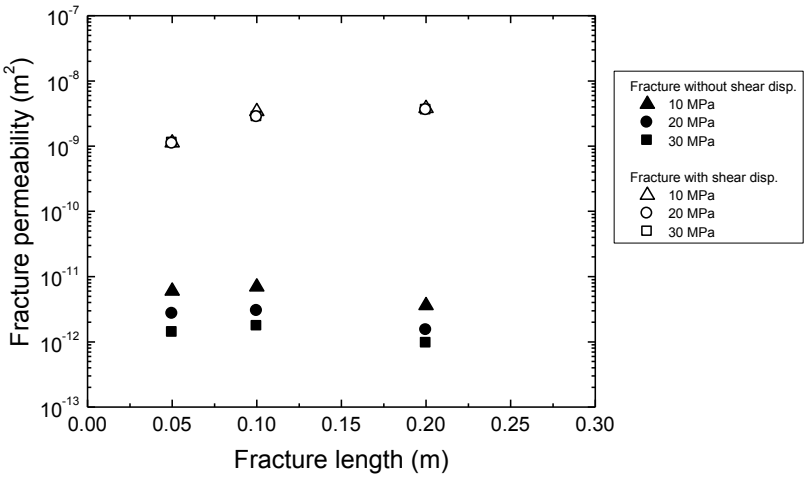

Figure 1: Changes in the fracture permeability with fracture length for real laboratory-scale fractures with no shear displacement and with a shear displacement of 5 mm at confining stresses of from 10 to 30 MPa.

Based on the measurements of the fracture permeability and surface topography, the fracture aperture distribution and the corresponding fluid flow are numerically determined for each given condition, indicating heterogeneous aperture distributions and the resulting channeling flows for all conditions. Figure 2 shows the representative results for channeling flows through the heterogeneous aperture distributions for the laboratory-scale fractures. In this figure, the flow rate distributions shown in color scale are superimposed on the corresponding aperture distributions, which are shown in gray scale. In Figure 2, the contacting asperities are represented by the minimum apertures of 1 μm for convenience, as described in Section 2.1. Moreover, the flow rates in each figure are normalized by the maximum flow rate for each condition, and flow rates of ≥ 0.01 (1% of the maximum flow rate) are shown in the figure. The distribution of the colored points therefore maps the dominant flow paths within the aperture distribution, because colorless points have negligibly small flow rates. As shown in the figure, in general, there are a significant number of nonzero aperture points that have a negligible flow rate, which demonstrates the formation of preferential flow paths (i.e., channeling flow).

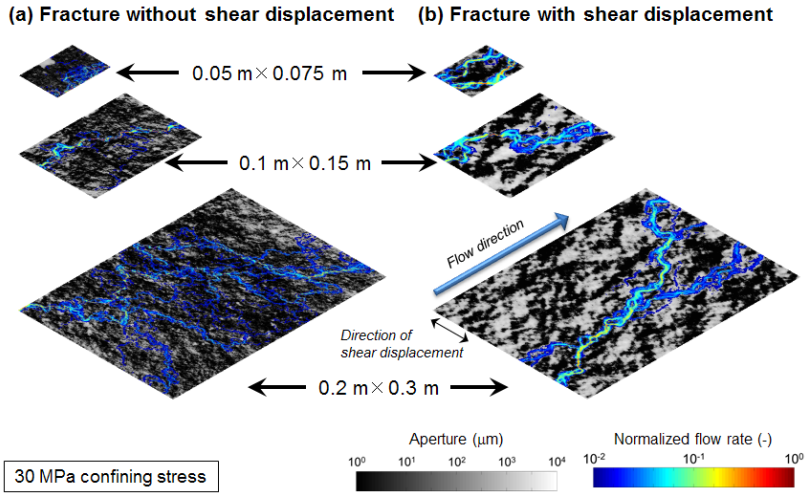

Figure 2: Representative results for the channeling flow within the heterogeneous aperture distribution of the real laboratory-scale fractures (a) with no shear displacement and (b) with a shear displacement of 5 mm.

Histograms of the aperture are generally characterized by a significant number of contacting asperities (regions of zero aperture) and the skewed distributions of regions of nonzero aperture with long tails, i.e., lognormal-like distributions, as reported in the literature (Watanabe et al., 2008 and 2009). Therefore, the aperture distributions are evaluated by the geometric mean and standard deviation of nonzero apertures and the percentage of zero apertures (contact area). Figure 3 shows the changes in the geometric mean of apertures, referred to hereinafter as the mean aperture, and the contact area with the respect to the fracture length. Due to the shear dilation, fractures with shear displacement generally have a large mean aperture. In addition, fractures without shear displacement have a large contact area due to the high degree of matedeness of the fracture surfaces. The mean aperture of the fracture without shear displacement, which does not change significantly with confining stress, increases with increasing fracture length. On the other hand, the mean aperture of the fracture with shear displacement, which does not change significantly with confining stress, first increases and then decreases with the increase in the fracture length. Since the mean aperture of the largest fracture remains greater than that of the smallest fracture, the mean aperture of the fracture with shear displacement essentially increases with increasing fracture length. The contact area of the fracture without shear displacement, which is slightly larger at higher confining stress, decreases slightly with the increase in the fracture length. In contrast, the contact area of the fracture with shear displacement, which does not change significantly with confining stress, increases slightly with increasing fracture length. The geometric standard deviations are essentially constant (approximately 3) for all given conditions.

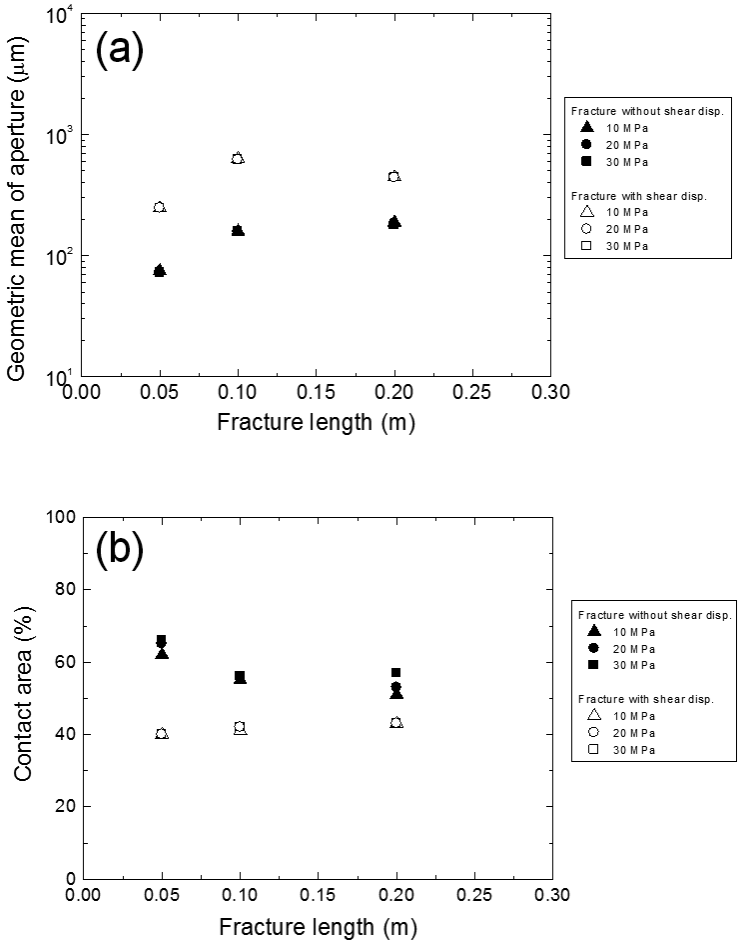

Figure 3: Changes in (a) the geometric mean of aperture and (b) the contact area for the real laboratory-scale fractures with no shear displacement and with a shear displacement of 5 mm at confining stresses of 10, 20, and 30 MPa.

The area of the preferential flow paths, referred to herein as the flow area, is calculated to evaluate the degree of channeling flow (Figure 4). For all of the given conditions, the flow area is far from 100% of the fracture plane, demonstrating the difference between reality and the fluid flow through a fracture modeled by parallel smooth plates. The fractures with shear displacement have a rather large flow area, except for the largest fracture, and this trend does not change significantly with confining stress. In the case of a fracture without shear displacement, the flow area is approximately constant throughout the tested fracture scales. On the other hand, the flow area of the fracture with shear displacement decreases slightly with the increase in the fracture length.

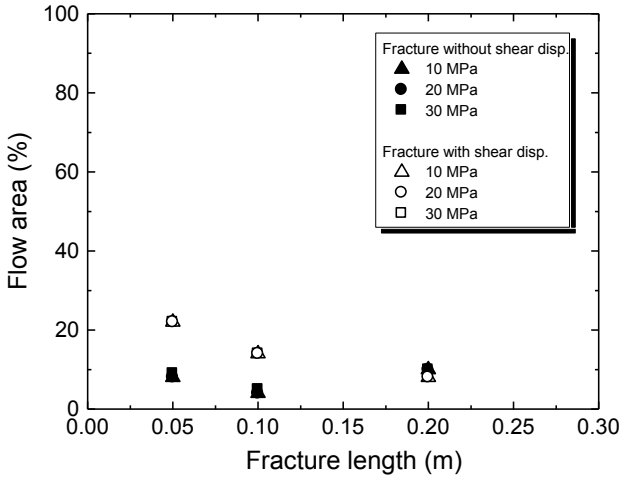

Figure 4: Changes in the flow area with the fracture length for the real laboratory-scale fractures with no shear displacement and a shear displacement of 5 mm at confining stresses of 10, 20, and 30 MPa.

Based on the above-described results, the scale dependencies of the heterogeneous fracture aperture distribution and the channeling flow therein are inferred as follows. For both fractures with and without shear displacement, the mean aperture increases with the increase in the fracture length, as demonstrated herein. This scale dependency of the mean aperture may be true because the fractal fracture surface has larger roughness at a larger fracture scale. In the laboratory scale, however, the mean aperture may not always

increase significantly with the increase in the fracture scale, due to the self-affinity, rather than self-similarity, of the fractal fracture surface. On the other hand, for both fractures with and without shear displacement, the contact area is virtually independent of scale. In the present study, the contact areas of the fractures with and without shear displacement exhibit opposite changes with respect to increasing fracture length. However, the changes in the absolute contact area are small and there is no reason for such opposite changes for these fractures. As such, these changes in the contact area are not essential, indicating the scale independency of the contact area. This concept has also been suggested in the literature (Witherspoon et al., 1979). The combination of the scale-dependent mean aperture and the scale-independent contact area suggests that the fracture permeability either remains constant or increases with the increase in the fracture length. In the case of a fracture without shear displacement, the permeability may remain approximately constant with the increase in the fracture length because the increase in the aperture has little influence on the permeability enhancement due to the large contact area. In contrast, for a fracture with shear displacement, the permeability may increase monotonically with the increase in the fracture scale due to the small contact area.

As described herein, the laboratory investigation provides insight into the scale dependencies of the aperture distributions and channeling flows for subsurface fractures. However, it is difficult to determine the scale dependencies due to the limited results for a relatively small range of fracture scale in the laboratory investigation. Therefore, a method by which to predict fracture aperture distributions beyond the laboratory scale has been developed based on the fractal nature and the scale-independent contact area of the fracture surface and has been used to address the prescribed problem.

3.2 Validity of the Method for Predicting Fracture Aperture Distributions beyond the Laboratory Scale

Fracture aperture distributions of the square fractures with side lengths of 0.05 to 0.6 m and the corresponding fluid flows are numerically determined by the prediction method, where the scale-independent contact areas of fractures with and without a shear displacement of 5 mm are set to 42% and 59%, respectively. These values can be obtained by calculating the average of contact area with respect to the fracture type, because the confining stress level has little influence on the contact area. Since the contact area and the other characteristic parameters do not change significantly with the confining stress, in the present study, the predicted aperture distributions and fluid flows can be considered to be representative of the fractures with and without shear displacement under confining stress.

In order to evaluate the validity of the prediction method, the occurrence of channeling flows within the predicted aperture distributions is first confirmed. In the same manner as in Figure 2, representative results for the aperture distribution and fluid flow are shown in Figure 5. Visual comparison of the distributions between the predicted fractures and the real, laboratory-scale fractures qualitatively reveals that the prediction method can reproduce the occurrence of a channeling flow within the heterogeneous fracture aperture distribution. The channeling flow for the predicted fractures beyond the laboratory scale of > 0.2 m × 0.3 m can also be observed, which suggests that this flow phenomenon generally characterizes the fluid flow through the rock fracture, regardless of scale. Quantitative evaluation of the validity of the prediction method is then conducted, primarily through the comparisons of two key parameters, namely, the mean aperture and the fracture permeability, between the predicted fractures and the real laboratory-scale fractures (Figure 6). The values of the mean aperture and permeability for the predicted fractures are generally in agreement with those of the real laboratory-scale fractures. Although relatively large differences are observed between the predicted and real permeabilities for the fracture without shear displacement, the differences are consistent within an order of magnitude. Moreover, the scale dependencies of the mean aperture and the permeability, which are observed in the laboratory investigation, are properly reproduced by the prediction method. Therefore, for both fractures with and without shear displacement, the mean aperture is expected to increase with the increase in the fracture length. In addition, the permeability of the fracture without shear displacement is almost scale-invariant, whereas the permeability of the fracture with shear displacement increases with the increase in the fracture length.

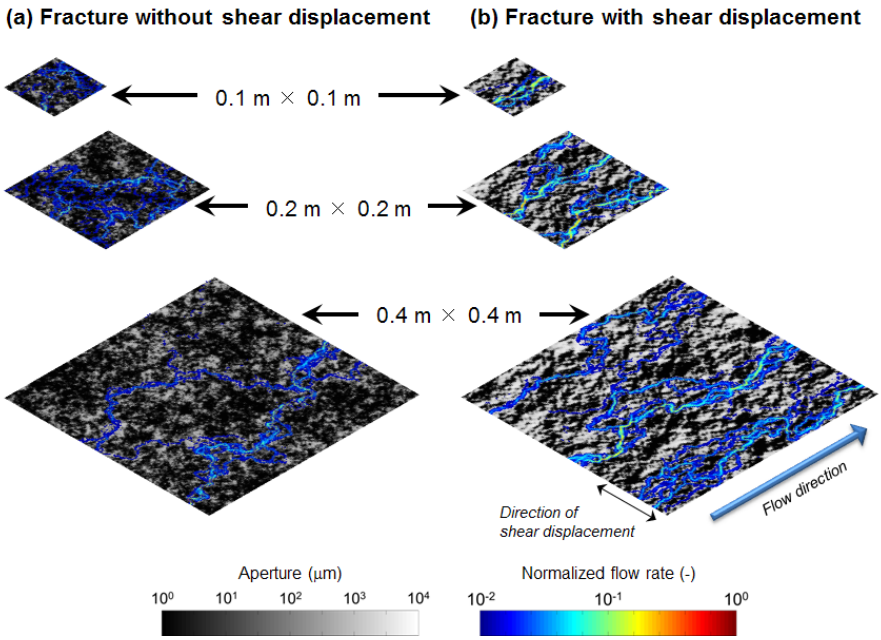

Figure 5: Representative results for the channeling flow within the heterogeneous aperture distribution of the predicted fractures (a) with no shear displacement and (b) with a shear displacement of 5 mm.

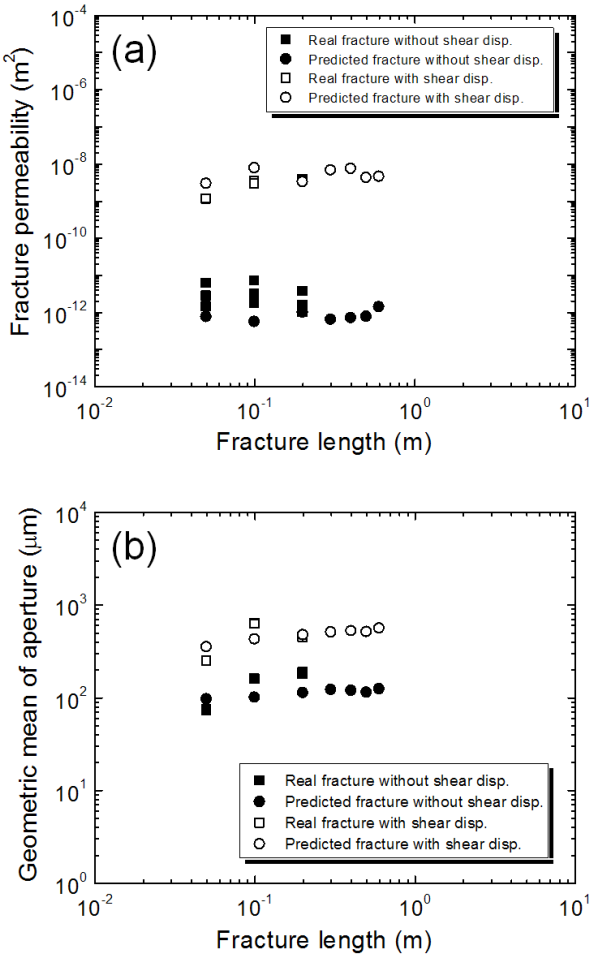

Figure 6: Comparisons of (a) the permeability and (b) the geometric mean of aperture between the predicted and the real laboratory-scale fractures with no shear displacement and with a shear displacement of 5 mm. The values for the real fractures are determined at confining stresses of 10, 20, and 30 MPa.

As described above, the prediction method has been demonstrated to be valid for fractures created in the laboratory. However, the validity of the prediction method for natural fractures is unclear. To address this concern, the maximum aperture-fracture length relations are obtained for the predicted fractures and are compared to those for natural fractures (joints and faults) reported in the literature (Cowie and Scholz, 1992; Vermilye and Scholz, 1995; Schlische et al., 1996; Schultz et al., 2008). Note that the maximum aperture in the present study corresponds to the maximum displacement in the literature. Vermilye and Scholz (1995) reported that the maximum aperture (m), e_{max}, and fracture length (m), l, are approximately related by the following formula:

$$e_{\max} = \alpha \cdot l^{n}, \tag{5}$$

where α is a pre-exponential factor related to rock properties or tectonic environments, and n is an exponent. In the case of a joint, the maximum aperture ranges from 10^{-4} m to 10^{-3} m for a fracture length ranging from 10^{-2} m to 1 m, and the representative fit curve is given as $e_{max} = 2.5\times10^{-3}l^{0.48}$ (Schultz et al., 2008). In contrast, in the case of a fault, the maximum aperture ranges from 10^{-4} m to 10^{5} m for a fracture length ranging from 10^{-3} m to 10^{6} m, which results in a pre-exponential factor of between 0.001 and 0.1 and an exponent of 1.

Figure 7 shows the maximum aperture-fracture length relations for the predicted fractures, together with those for joints and faults in nature. In addition to the results for the fractures with no shear displacement and a shear displacement of 5 mm, the results for fractures with a constant ratio of shear displacement to fracture length are shown in Figure 7. In the present study, the results for the fractures with and without shear displacement are compared to those for faults and joints, respectively. However, whether the fractures with a shear displacement of 5 mm are suitable for the comparison remains unclear, because the shear displacement of a fault generally exhibits a linear increase with respect to the fracture scale (Kanamori and Anderson, 1975). Consequently, a constant ratio of shear displacement to fracture length is also used. Here, a relatively large ratio of 0.01 (1% of the fracture length) is assumed because most faults are expected to experience multiple slips, rather than just a single slip. As shown in Figure 7, the maximum aperture-fracture length relation for the fracture without shear displacement quantitatively coincided with that for the joint ($e_{max} = 2.5\times10^{-3}l^{0.48}$). Furthermore, the maximum aperture-fracture length relation for the fracture with a constant ratio of shear displacement is quantitatively consistent with the middle relation for the fault ($e_{max} = 0.01l$), whereas the maximum aperture-fracture length relation for a fracture with a constant shear displacement is inconsistent with the relations for natural faults, which is as expected. Thus, the prediction method has also been demonstrated to be valid for natural fractures (joints and faults).

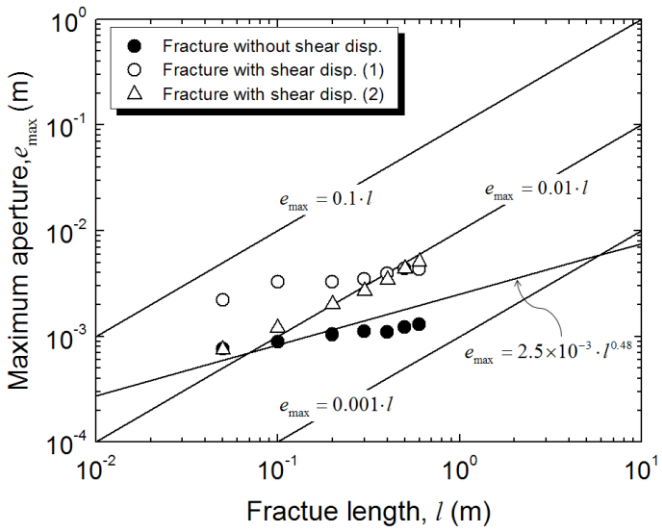

Figure 7: Comparison of the maximum aperture-fracture length relations between the predicted and the natural fractures. The results are for the predicted fractures with two types of shear displacement: (1) a constant shear displacement of 5 mm and (2) a shear displacement that is a constant 1% of the fracture length. One of the linear curves, $e_{max} = 2.5\times10^{-3}l^{0.48}$, corresponds to the relation of the joint, whereas the other linear curves correspond to the relations of the fault (Schlische et al., 1996; Schultz et al., 2008).

3.3 Scale Dependency of a Channeling Flow through a Heterogeneous Fracture Aperture Distribution

Since the prediction method has been demonstrated to be valid for natural fractures, the present study finally discusses conceivable scale dependencies of channeling flows through the heterogeneous aperture distributions of natural fractures, i.e., joints and faults. Considering the above discussion, we assume that the prediction results for fractures without shear displacement are relevant to the typical scale dependencies of joints, whereas the prediction results for the fractures with a constant ratio of shear displacement are relevant to the typical scale dependencies of faults.

Figure 8a shows the changes in the mean aperture with the fracture length for both fractures with and without shear displacement, which are hereinafter referred to as faults and joints, respectively. For both joints and faults, the mean aperture increases with the increase in the fracture length, whereas the standard deviation is almost independent of scale and is approximately 3. The increase in the mean apertures may have occurred because the fracture surface becomes rougher with the increase in the fracture length and the contact area is a scale-independent value. The increase in mean aperture for joints and faults are linear on a log-log plot, and are respectively approximated by

$$e_{m,joint} = 1\times10^{2} \cdot l^{0.1}, \tag{6}$$

$$e_{m,fault} = 1\times10^{3} \cdot l^{0.7}, \tag{7}$$

where $e_{m,\ joint}$ and $e_{m,\ fault}$ are the mean apertures (μm) of joints and faults, respectively, and l is the fracture length (m). Both equations have exponents smaller than unity due to the self-affine fractal nature of the fracture surface. In particular, the exponent is very small for the joint, indicating the weak scale dependency of the mean aperture. The small exponent is due to the high degree of matedness for the two opposite fracture surfaces.

Figures 8b and 8c show the change in permeability and flow area with fracture length for joints and faults. The permeabilities of both joints and faults also increase linearly with fracture length on a log-log plot and are approximated by

$$k_{joint} = 1\times10^{-12} \cdot l^{0.2}, \tag{8}$$

$$k_{fault} = 1\times10^{-8} \cdot l^{1.1}, \tag{9}$$

where k_{joint} and k_{fault} are the permeabilities (m^2) of joints and faults, respectively. For both joints and faults, the exponents for the permeability are greater than those of the mean aperture. The permeabilities have stronger scale dependencies than those of the mean apertures, because the local permeabilities are proportional to the square of the local apertures (i.e., local cubic law). However, the pre-exponential factors and exponents in Equations 8 and 9 are smaller than those expected from Equations 6 and 7 with an assumption of the parallel smooth plate model, where the fracture permeability is proportional to the square of the mean aperture. This is because the flow area within a fracture is quite small due to the channeling flow, as shown in Figure 8c, which diverges significantly from the assumption. Due to the significantly small exponent for the joint, the permeability is approximately constant with respect to the fracture scale. Note that Equations 6 through 9 may be used to predict the fracture flow characteristics for a confining stress of up to approximately 100 MPa. This constraint can be inferred from the study of Watanabe et al. (2008), who showed that the change in the fluid flow characteristics of the fracture is relatively small with an increase in confining stress of from 30 MPa to 100 MPa. In contrast, for both joints and faults, the flow area is virtually independent of scale and is approximately

10% of the fracture plane. Considering the scale-independent contact area of approximately 60% for joints and 40% for faults, we assume the existence of a noncontact area that does not contribute to the fluid flow for both joint and fault planes. The noncontact areas (i.e., a stagnant area of fluid) of joints and faults, which are also scale-independent values, are estimated to be approximately 30% and 50%, respectively. The estimated flow area within the fracture plane corresponds well with the flow area evaluated through field investigations (Abelin et al., 1985).

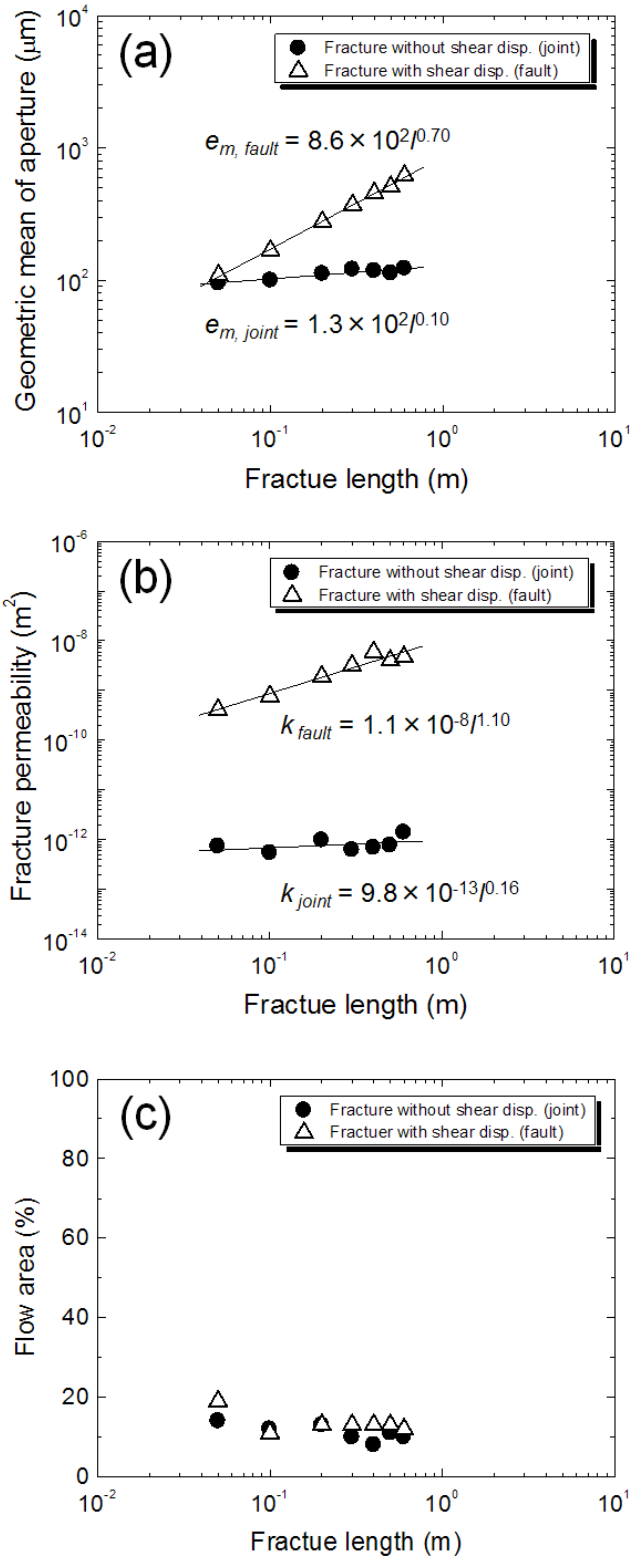

Figure 8: Predicted typical changes in the (a) geometric mean of aperture, (b) the permeability, and (c) the flow area, all with respect to the fracture length, for fractures with no shear displacement (joints) and fractures with a constant ratio of shear displacement to fracture length (faults).

4. CONCLUSIONS

We evaluated heterogeneous aperture distributions and resulting channeling flows for granite fractures of various sizes under confining stress. As a significant result, the scale independency of contact area of the fracture was revealed, which, in combination with the well-known fractal nature of the fracture surfaces, provides a novel method by which to predict fracture aperture distributions beyond the laboratory scale. The validity of the proposed method was revealed through the reproduction of the results in a laboratory investigation and the maximum aperture-fracture length relations, which have been reported in the literature, for natural fractures (i.e., joints and faults).

Subsequently, for joints and faults of various sizes, representative aperture distributions and resulting channeling flows were numerically determined under confining stress. The characteristics of the aperture distributions and the fluid flow were evaluated, and the changes in the mean aperture and permeability with the fracture scale were formulated. Therefore, we can now predict conceivable scale dependencies of channeling flows through heterogeneous aperture distributions from laboratory-scale to field-scale natural fractures.

In summary, these results are essential to the design of fracture networks with scale-dependent heterogeneous aperture distributions in the field scale. Such precise analysis of a fracture network will provide new insight into transport phenomenon within a fracture network, which will have significant engineering and scientific applications, such as in the development of geothermal or hydrocarbons reservoirs.

ACKNOWLEDGEMENTS

The present study was supported in part by the Japan Society for the Promotion of Science (JSPS) through a Grant-in-Aid for JSPS Fellows (24-3097), and a Grant-in-Aid for Specially Promoted Research, No. 25000009.

REFERENCES

Abelin, H., Neretnieks, I., Tunbrant, S., and Moreno, L.: Migration in a single fracture: Experimental results and evaluation, final report, Stripa Project, Stockholm, Sweden, May 1985, (1985).

Berkowitz, B.: Characterizing flow and transport in fractured geological media: A review, *Adv. Water Resour.*, **25**, (2002), 861-884.

Brown, S. R.: A note on the description of surface roughness using fractal dimension, *Geophys. Res. Lett.*, **14**, (1987a),1095-1098.

Brown, S. R.: Fluid flow thorough rock joints: The effect of surface roughness, *J. Geophys. Res.*, **92**(B2), (1987b),1337-1347.

Brown, S. R.: Transport of fluid and electric current through a single fracture, *J. Geophys. Res.*, **100**(B7), (1989), 9429-9438.

Brown, S. R.: Simple mathematical model of a rough fracture, *J. Geophys. Res.*, **100**(B4), (1995), 5941-5952.

Brown, S. R., Stockman, H. W., and Reeves, S. J.: Applicability of Reynolds equation for modeling fluid flow between rough surfaces, *Geophys. Res. Lett.*, **22**(18), (1995), 2537-2540.

Brown, S., Caprihan, A., and Hardly, R.: Experimental observation of fluid flow channels in a single fracture, *J. Geophys. Res*., **103**(B3), (1998), 5125-5132.

Brush, D. J., and Thomson, N. R.: Fluid flow in synthetic rough-walled fractures: Navier-Stokes, Stokes, and local cubic law assumptions, *Water Resour. Res.*, **39**(4), (2003), 1085, doi:10.1029/2002WR001346.

Candela, T., Renard, F., Klinger, Y., Mair, K., Schmittbuhl, J., and Brodsky, E. E.: Roughness of fault surfaces over nine decades of length scales, *J. Geophys. Res*., **117**, (2012), B08409, doi:10.1029/2011JB009041.

Cowie, P. A., and Scholz, C. H.: Displacement-length scaling relationship for faults: data synthesis and discussion, *J. Struct. Geol*., **14**(10), (1992), 1149-1156.

Dreuzy, J. R., Méheust, Y., and Pichot, G.: Influence of fracture scale heterogeneity on the flow properties of three-dimensional discrete fracture networks (DFN), *J. Geophys. Res*., **117**, (2012), B11207, doi:10.1029/2012JB009461.

Durham, W. B.: Laboratory observations of the hydraulic behavior of a permeable fracture from 3800 m depth in the KTB pilot hole, *J. Geophys. Res*., **102**(B8), (1997), 18,405-18,416.

Ge, S.: A governing equation for fluid flow in rock fractures, *Water Resour. Res*., **33**(1), (1997), 53-61.

Glover, P. W. J., Matsuki, K., Hikima, R., and Hayashi, K.: Fluid flow in fractally rough synthetic fractures, *Geophys. Res. Lett*., **24**(14), (1997), 1830-1806.

Glover, P. W. J., Matsuki, K., Hikima, R., and Hayashi, K.: Synthetic rough fractures in rocks, *J. Geophys. Res*., **103**(B5), (1998), 9609-9620.

Ishibashi, T., Watanabe, N., Hirano, N., Okamoto, A., and Tsuchiya, N.: GeoFlow: A novel model simulator for prediction of the 3-D channeling flow in a rock fracture network, *Water Resour. Res*., **48**, (2012), W07601, doi:10.1029/2011WR011226.

Jaeger, J. C., Cook, N. G. W., and Zimmerman, R. W.: Fundamentals of rock mechanics, Wiley-Blackwell. (2007),

Jing, Z., Richards, J. W., Watanabe, K., and Hashida, T.: A three-dimensional stochastic rock mechanics model of engineered geothermal systems in fractured crystalline rock, *J. Geophys. Res*., **105**(B10), (2000), 23663-23679.

Kanamori, H., and Anderson, D. L.: Theoretical basis of some empirical relations in seismology, *Bull. Seism. Soc. Am.*, **65**(5), (1975), 1073-1095.

Kumar, S., and Bodvarsson, G. S.: Fractal study and simulation of fracture roughness, *Geophys. Res. Lett.*, **17**(6), (1990), 701-704.

Long, J. C. S., Remer, J. S., Wilson, C. R., and Witherspoon, P. A.: Porous media equivalents for networks of discontinuous fractures, *Water Resour. Res.*, **18**(3), (1982), 645-658.

Matsuki, K., Chida, Y., Sakaguchi, K., and Glover, P. W. J.: Size effect on aperture and permeability of a fracture as estimated in large synthetic fractures, Int. J. Rock Mech. Min. Sci., 43(5), (2006), 726-755.

Min, K. B., Rutqvist, J., Tsang, C. -F., and Jinga, L.: Stress-dependent permeability of fractured rock masses: a numerical study, *Int. J. Rock Mech. Min. Sci*., **41**, (2004), 1191-1210.

Nemoto, K., Watanabe, N., Hirano, N., and Tsuchiya, N.: Direct measurement of contact area and stress dependence of anisotropic flow through rock fracture with heterogeneous aperture distribution, *Earth Planet. Sci. Lett*., **281**, (2009), 81-87.

Neuman, S. P.: Trends, prospects and challenges in quantifying flow and transport through fractured rocks, *Hydrogeol. J.*, **13**(1), (2005), 124-147, doi:10.1007/s10040-004-0397-2.

Oron, A. P., and Berkowitz, B.: Flow in rock fractures: The local cubic law assumption reexamined, *Water Resour. Res*., **34**(11), (1998), 2811-2825.

Power, W. L., Tullis, T. E., Brown, S. R., Boitnott, G. N., and Scholz, C. H.: Roughness of natural fault surfaces, *Geophys. Res. Lett.*, **14**(1), (1987), 29-32, doi:10.1029/GL014i001p00029.

Power, W. L., and Durham, W. B.: Topography of natural and artificial fractures in granitic rocks: Implications for studies of rock friction and fluid migration, *Int. J. Rock Mech. Min. Sci.*, **34**(6), (1997), 979-989.

Pyrak-Nolte, L. J., Cook, N. G. W., and Nolte, D. D.: Fluid percolation through single fractures, *Geophys. Res. Lett.*, **15**(11), (1988), 1247-1250.

Raven, K. G., and Gale, J. E.: Water flow in natural rock fracture as a function of stress and sample size, *Int. J. Rock Mech. Min. Sci*., **22**(4), (1985), 251-261.

Sausse, J. Hydromechanical properties and alteration of natural fracture surfaces in the Soultz granite (Bas-Rhin, France), *Tectonophysics*, **348**(1), (2002), 169-185.

Schlische, R. W., Young, S. S., Ackermann, R. V., and Gupta. A.: Geometry and scaling relations of a population of very small rift-related normal faults, *Geology*, **24**(8), (1996), 683-686.

Schultz, R. A., Soliva, R., Fossen, H., Okubo, C. H., and Reeves, D. M.: Dependence of displacement-length scaling relations for fractures and deformation bands on the volumetric changes across them, *J. Struct. Geol*., **30**, (2008), 1405-1411.

Talon, L., Auradou, H., and Hansen, A.: Permeability estimates of self-affine fracture faults based on generalization of the bottle neck concept, *Water Resour. Res.*, **46**, (2010), W07601, doi:10.1029/2009WR008404.

Tsang, C. F., and Neretnieks, I.: Flow channeling in heterogeneous fractured rocks, *Rev. Geophys*., **36**, (1998), 275-298.

Tsang, Y. W., and Witherspoon, P. A.: Hydromechanical behavior of a deformable rock fracture subject to normal stress, *J. Geophys. Res.*, **86**(B10), (1981), 9287-9298.

Vermilye, J. M., and Scholz, C. H.: Relation between vein length and aperture, *J. Struct. Geol.*, **17**(3), (1995), 423-434.

Watanabe, N., Hirano, N., and Tsuchiya, N.: Determination of aperture structure and fluid flow in a rock fracture by high-resolution numerical modeling on the basis of a flow-thorough experiment under confining pressure, *Water Resour. Res.*, **44**, (2008), W06412, doi:10.1029/2006WR005411.

Watanabe, N., Hirano, N., and Tsuchiya, N.: Diversity of channeling flow in heterogeneous aperture distribution inferred from integrated experimental-numerical analysis on flow through shear fracture in granite, *J. Geophys. Res*., **114**, (2009), B04208, doi:10.1029/2008JB005959.

Watanabe, N., Ishibashi, T., Hirano, N., Tsuchiya, N., Ohsaki, Y., Tamagawa, T., Tsuchiya, Y., and Okabe, H.; Precise 3D numerical modeling of fracture flow coupled with X-ray Computed tomography for reservoir core samples, *SPE J.*, **16**(3), (2011a), 683-691, doi:10.2118/146643-PA.

Watanabe, N., Ishibashi, T., Ohsaki, Y., Tsuchiya, Y., Tamagawa, T., Hirano, N., Okabe, H., and Tsuchiya N.: X-ray CT based numerical analysis of fracture flow for core samples under various confining pressure, *Eng. Geol.*, **123**, (2011b), 338-346, doi:10.1016/j.enggeo.2011.09.010.

Watanabe, N., T. Ishibashi, N. Tsuchiya, Y. Ohsaki, T. Tamagawa, Y. Tsuchiya, H. Okabe, H. Ito (2012), Geologic core holder with CFR PEEK body for the X-ray CT based numerical analysis of fracture flow under confining pressure, *Rock Mech. Rock Eng.*, **46**(2), 413-418, doi:10.1007/s00603-012-0311-5.

Witherspoon, P. A., C. J. Amick, J. E. Gale, and K. Iwai (1979), Observations of a potential size effect in experimental determination of the hydraulic properties of fractures, *Water Resour. Res*., **15**(5), 1142-1146.

Witherspoon, P. A., J. S. Y. Wang, K. Iwai, and J. E. Gale (1980), Validity of cubic law for fluid flow in a deformable rock fracture, *Water Resour. Res*., **16**(6), 1016-1024.

Yeo, I. W., M. H. de Freitas, and R. W. Zimmerman (1998), Effect of shear displacement on the aperture and permeability of a rock fracture, *Int. J. Rock Mech. Min. Sci.*, **35**(8), 1051-1070.

Zimmerman, R. W., D. W. Chen, and N. G. W. Cook (1992), The effect of contact area on the permeability of fractures, *J. Hydrol.,* **139**, 79-96.